Error bounds for variational quantum time evolution

Author(s):
Zoufal, Christa (iD); Sutter, David (iD); Woerner, Stefan

Error bounds for variational quantum time evolution

Christa Zoufal[1,2,*] David Sutter[1] and Stefan Woerner[1]

[1] *IBM Quantum, IBM Research Europe – Zurich, Switzerland*
[2] *Institute for Theoretical Physics, ETH Zurich, Switzerland*

Variational quantum time evolution allows us to simulate the time dynamics of quantum systems with near-term compatible quantum circuits. Due to the variational nature of this method the accuracy of the simulation is *a priori* unknown. We derive *a posteriori* global phase agnostic error bounds for the state simulation accuracy with variational quantum time evolution that improve the tightness of fidelity estimates over existing *a posteriori* error bounds. These analysis tools are practically crucial for assessing the quality of the simulation and making informed choices about simulation hyperparameters. The efficient, *a posteriori* evaluation of the bounds can be tightly integrated with the variational time simulation and, hence, results in a minor resource overhead, which is governed by the system's energy variance. The performance of the error bounds is demonstrated on numerical examples.

I. INTRODUCTION

Quantum time evolution (QTE) generally describes the process of evolving a quantum state over time with respect to a Hamiltonian H. In quantum real-time evolution (QRTE), which is BQP-complete [1], a state is evolved according to unitary quantum dynamics of the form $e^{-iHt/\hbar}$ for $t \in \mathbb{R}$, e.g., simulating many-body dynamics [2–4]. If the time parameter t is replaced by an imaginary time $\tau = -it$ the system dynamics change to a nonunitary quantum imaginary time evolution (QITE) $e^{-H\tau/\hbar}$, which is believed to be QMA-hard [5]. Hence, even a quantum computer is not expected to enable an efficient and exact execution of a generic form of these dynamics but might only perform well for certain instances. Finding these instances, or approximations thereof, is of great interest as QITE has many practically relevant applications. Suppose that the initial state has a nonzero overlap with the ground state of H, then all components that do not correspond to the ground state are damped exponentially in time during imaginary time evolution. This form of time evolution is, thus, a particularly useful tool to find the ground state of H [6]. Furthermore, imaginary time evolution can be used to solve partial differential equations [7,8], to prepare

quantum Gibbs states [9–13], or to solve combinatorial optimization problems [14].

In order to implement QTE on an actual quantum computer, the time evolution must be translated into a hardware native process. Thus, quantum simulation on a gate-based quantum computer requires a translation into quantum gates, which may, e.g., be approximated with Trotterization [11,15]. While this approach has many advantages, the resulting quantum circuits can easily become too deep for reliable execution on near-term devices. *Variational quantum time evolution* (VarQTE) [6,10,16,17] offers an interesting alternative that can simulate quantum time dynamics with (shallow) parameterized quantum circuits. Next to its compatibility with shallow, variational quantum circuits, the method's ability to offload parts of the algorithmic calculations to classical computers makes it a promising candidate for solving interesting QTE problems with near-term devices. However, VarQTE does rely on a variational approximation and, hence, generally comes with an approximation error. The efficient quantification of this error is crucial to allow for interpretation of the results, and to possibly adapt the simulation setting, respectively, the chosen methodological hyperparameters.

Error bounds for algorithmic and implementation induced errors of variational quantum real-time evolution (VarQTE) given by the time-dependent variational principle [18] with respect to the trace distance D_{Tr} are introduced in Ref. [16]. The respective bound depends on the operator norm of H^2, which usually scales unfavorably. This issue is resolved in a consecutive work presented in Ref. [17] where efficient error bounds for the variational simulations of general processes—including

---

*ouf@zurich.ibm.com

$$D_{\text{Tr}} \le B \le \ell_2$$
$$\hspace{0.5cm} |\wedge \hspace{0.6cm} |\wedge$$
$$\epsilon \le \epsilon^{\text{PD}}$$

FIG. 1. This figure illustrates the inequality relations between the distance metrics and algorithmic error bounds that have been considered in related work, respectively, are being considered in this work.

VarQRTE and variational quantum imaginary time evolution (VarQITE)—are derived for the trace distance. Furthermore, Ref. [19] introduces an error bound ϵ^{PD} for the ℓ_2-norm between target state and state prepared with VarQRTE based on McLachlan's variational principle [20] that suffers from global phase dependence. Interestingly, the algorithmic error bound for VarQRTE presented in Ref. [17] is equivalent to the bound from Ref. [19], i.e., ϵ^{PD}.

In this work, we introduce *a posteriori* error bounds ϵ for VarQRTE and VarQITE based on the Bures distance B, which is agnostic to physically irrelevant global phase mismatches—a feature that is aligned with the theory of state-of-the-art implementations [6]. These error bounds are an important progress towards practical quantum simulation verification for VarQTE. More specifically, the obtained error bounds enable us to efficiently quantify the algorithmic approximation error with respect to the optimal QTE solution. Most quantities are already known from the variational principle itself. The additionally required resources to evaluate the bounds are at most quadratically more expensive in the number of Hamiltonian terms. A discussion on the resource overhead can be found in Appendix A. Furthermore, the bounds are practically easy to implement through numerical integration of an ordinary differential equation (ODE) that is defined by residual quantities stemming from the underlying variational equations. Moreover, the alternative error bounds ϵ define lower bounds on the phase-dependent ϵ^{PD} from Refs. [17,19] and on the fidelity between prepared and target states due to a direct relation of the Bures metric to the fidelity. It should also be noted that the Bures metric upper bounds the trace distance. The Bures metric and ℓ_2-norm as well as ϵ and ϵ^{PD} are trivially equivalent if the time evolution does not introduce a global phase change or the variational ansatz manages to perfectly capture the global phase change. The equivalence between trace distance and Bures metric, on the other hand, holds only if the underlying states are equal up to global phase, i.e., if they are zero. Otherwise, the inequality becomes strict. It directly follows that we can also derive a bound on D_{Tr} using ϵ that is strictly better than ϵ^{PD}. The inequality relations of the various metrics and respective error bounds are illustrated in Fig. 1 and discussed in more detail in Appendix B.

Our main contributions of this work are summarized as follows: Firstly, this work presents improved algorithmic error bounds ϵ for VarQTE implementations that are based on McLachlan's variational principle that lower bound existing bounds ϵ^{PD} [17,19]. We discuss practically relevant aspects considering the integration of the ODE underlying VarQTE. Lastly, the practical behavior of the error bounds is demonstrated on various numerical examples. We investigate their performance and illustrate the application to concrete settings.

The structure of this work is as follows. First, we explain the concepts of (variational) quantum time evolution in Sec. II. Then, Sec. III introduces the *a posteriori* error bounds for VarQRTE and VarQITE. Furthermore, methods used for the numerical experiments are described in Sec. IV A and the respective results are presented in Sec. IV. Finally, conclusions and outlook are given in Sec. V.

II. VARIATIONAL QUANTUM TIME EVOLUTION

VarQTE maps the time evolution of a state $|\psi_t^*\rangle$ onto a variational ansatz state $|\psi_t^\omega\rangle$ whose time dependence is projected onto the parameters $\boldsymbol{\omega_t}$. To simplify the notation, the time parameter t is dropped from $\boldsymbol{\omega} = (\omega_0, \ldots, \omega_k) \in \mathbb{R}^{k+1}$ in the remainder of this work when referring to the ansatz parameters. More specifically, we consider the current state-of-the-art formulation for pure states based on McLachlan's variational principle [20] with a global phase agnostic evolution [10]. This formulation directly compensates for terms that arise if the global phase of the state changes during the time evolution. While the global phase is physically irrelevant, it can lead to erroneous propagation dynamics if not being attributed for appropriately.

The state evolution described by the variational principle corresponds to an initial value problem where the underlying *ordinary differential equation* [21] is derived from McLachlan's variational principle [20]. We simulate the time evolution by numerically solving the ODE for a set of initial parameter values. It should be noted that the respective formulation not only enables QTE simulations for Hamiltonians given as a weighted sum of Pauli operators but also for Hamiltonians, which are incompatible with Trotterization such as those given in first quantization [22]. In the following, the real and imaginary time evolution, as well as, the variational implementations are introduced. Notably, we set without loss of generality $\hbar = 1$.

A. Variational quantum real-time evolution

The time-dependent Schrödinger equation describes the change of a state $|\psi_t^*\rangle$ under real-time evolution

$$i |\dot{\psi}_t^*\rangle = H |\psi_t^*\rangle, \tag{1}$$

where we use the time-derivative notation

$$\dot{a} = \frac{\partial a}{\partial t}. \tag{2}$$

The resulting time-dependent state reads

$$|\psi_t^*\rangle = e^{-iHt} |\psi_0^*\rangle. \tag{3}$$

The variational approximation of $|\psi_t^*\rangle$ with $|\psi_t^\omega\rangle$ is based on the ODE defined by

$$\sum_{j=0}^{k} \mathcal{F}_{ij}^{Q} \dot{\omega}_j = \mathrm{Im}\left(C_i - \frac{\partial \langle \psi_t^\omega|}{\partial \omega_i} |\psi_t^\omega\rangle E_t^\omega\right), \tag{4}$$

where $C_i = \frac{\partial \langle \psi_t^\omega|}{\partial \omega_i} H |\psi_t^\omega\rangle$, $E_t^\omega = \langle \psi_t^\omega| H |\psi_t^\omega\rangle$, and $\mathcal{F}_{ij}^{Q}$ denotes the (i,j) entry of the Fubini-Study metric [23,24] given by

$$\mathcal{F}_{ij}^{Q} = \mathrm{Re}\left(\frac{\partial \langle \psi_t^\omega|}{\partial \omega_i} \frac{\partial |\psi_t^\omega\rangle}{\partial \omega_j} - \frac{\partial \langle \psi_t^\omega|}{\partial \omega_i} |\psi_t^\omega\rangle\langle \psi_t^\omega| \frac{\partial |\psi_t^\omega\rangle}{\partial \omega_j}\right).$$

Practically, solving Eq. (4) can be reformulated as a minimization problem of the form

$$f_{\mathrm{res}}(\boldsymbol{\omega}) = \underset{\dot{\boldsymbol{\omega}} \in \mathbb{R}^{k+1}}{\mathrm{argmin}} \left\| \mathcal{F}^{Q}\dot{\boldsymbol{\omega}} - \mathrm{Im}\left(\boldsymbol{C} - \frac{\partial \langle \psi_t^\omega|}{\partial \boldsymbol{\omega}} |\psi_t^\omega\rangle E_t^\omega\right)\right\|, \tag{5}$$

with $\boldsymbol{C} = (C_0, \ldots, C_k)$. Alternatively, Eq. (4) could also be solved via pseudoinversion or even exact inversion if $\mathcal{F}^Q$ is invertible.

We would like to point out that for pure states the Fubini-Study metric is proportional to the quantum Fisher information matrix. The derivation of the global phase agnostic form of the VarQRTE ODE given in Eq. (4) is presented in Appendix C and the efficient evaluation of the respective terms is discussed in Appendix G. Due to the variational approximation, the gradient $|\dot{\psi}_t^{\dot{\nu}}\rangle$ will typically not be exact and, hence, $\| |e_t\rangle \| > 0$ for

$$|e_t\rangle := |\dot{\psi}_t^{\dot{\nu}}\rangle + iH |\psi_t^\omega\rangle \tag{6}$$

denoting the gradient error or residual of a single VarQRTE step.

We may also consider our problem from a different angle. Instead of considering Eq. (5), we may also look

for the argument $\dot{\boldsymbol{\omega}}$, which minimizes the residual, i.e.,

$$f_{\mathrm{err}}(\boldsymbol{\omega}) = \underset{\dot{\boldsymbol{\omega}} \in \mathbb{R}^{k+1}}{\mathrm{argmin}} \| |e_t\rangle \|_2^2, \tag{7}$$

where

$$\| |e_t\rangle \|_2^2 = \mathrm{Var}(H)_{\psi_t^\omega} + \left(\langle \dot{\psi}_t^\omega|\dot{\psi}_t^\omega\rangle - \langle \dot{\psi}_t^\omega|\psi_t^\omega\rangle \langle \psi_t^\omega|\dot{\psi}_t^\omega\rangle\right)$$
$$- 2\mathrm{Im}\left(\langle \dot{\psi}_t^\omega| H |\psi_t^\omega\rangle - E_t^\omega \langle \dot{\psi}_t^\omega|\psi_t^\omega\rangle\right), \tag{8}$$

for $\mathrm{Var}(H)_{\psi_t^\omega} = \langle \psi_t^\omega| H^2 |\psi_t^\omega\rangle - (E_t^\omega)^2$ and $2\mathrm{Re}(\langle \psi_t^\omega|\dot{\psi}_t^\omega\rangle) = \partial \langle \psi_t^\omega|\psi_t^\omega\rangle / \partial t = 0$. The minimization of an error of this form—neglecting the phase factors—is also employed in Ref. [25] to pick which coefficients and Pauli terms to include in a product formula based time-evolution state approximation.

Since the time dependence of $|\psi_t^\omega\rangle$ is encoded in the real parameters $\boldsymbol{\omega}$, Eq. (8) can be further rewritten as

$$\| |e_t\rangle \|_2^2 = \mathrm{Var}(H)_{\psi_t^\omega} + \sum_{i,j} \dot{\omega}_i\dot{\omega}_j \mathcal{F}_{ij}^{Q}$$
$$- 2\sum_{i} \dot{\omega}_i \mathrm{Im}\left(C_i - \frac{\partial \langle \psi_t^\omega|}{\partial \omega_i} |\psi_t^\omega\rangle E_t^\omega\right) \tag{9}$$

using

$$\mathrm{Im}\left(\langle \dot{\psi}_t^\omega| H |\psi_t^\omega\rangle - E_t^\omega \langle \dot{\psi}_t^\omega|\psi_t^\omega\rangle\right)$$
$$= \sum_{i} \dot{\omega}_i \mathrm{Im}\left(C_i - \frac{\partial \langle \psi_t^\omega|}{\partial \omega_i} |\psi_t^\omega\rangle E_t^\omega\right) \tag{10}$$

and

$$\langle \dot{\psi}_t^\omega|\dot{\psi}_t^\omega\rangle - \langle \dot{\psi}_t^\omega|\psi_t^\omega\rangle \langle \psi_t^\omega|\dot{\psi}_t^\omega\rangle = \sum_{i,j} \dot{\omega}_i\dot{\omega}_j \mathcal{F}_{ij}^{Q}. \tag{11}$$

All terms required to compute $\| |e_t\rangle \|_2$ can be evaluated with the techniques presented in Appendix G.

We would like to point out that the solutions to Eqs. (5) and (7) are analytically equivalent but the numerical behavior may differ. More specifically, the simulation results presented in Sec. IV present a more stable behavior of the latter.

B. Variational quantum imaginary time evolution

Imaginary time evolution of a quantum state is mathematically described by the normalized, Wick-rotated Schrödinger equation

$$|\dot{\psi}_t^*\rangle = \left(E_t^* \mathbb{1} - H\right) |\psi_t^*\rangle, \tag{12}$$

where $E_t^* = \langle \psi_t^*| H |\psi_t^*\rangle$ corresponds to the system energy. In the remainder of this work, the notation for

$E_t^* \mathbb{1} - H$ is simplified to $E_t^* - H$. The state evolution reads

$$|\psi_t^*\rangle = \frac{\mathrm{e}^{-Ht} |\psi_0^*\rangle}{\sqrt{\langle \psi_0^* | \, \mathrm{e}^{-2Ht} \, | \psi_0^* \rangle}}. \qquad (13)$$

Analogously to Sec. II A, we simulate the existence of an explicit global phase $\mathrm{e}^{-i\nu}$ [6,10] and, thereby, avoid the addition of a physically irrelevant phase gate.

Solving

$$\sum_{j=0}^{k} \mathcal{F}_{ij}^{Q} \dot{\omega}_j = -\mathrm{Re}\left(C_i\right), \qquad (14)$$

for $\dot{\boldsymbol{\omega}}$ leads to an ODE, which describes the evolution of the ansatz parameters in terms of the parameter updates that minimize

$$f_{\mathrm{res}}\left(\boldsymbol{\omega}\right) = \underset{\dot{\boldsymbol{\omega}} \in \mathbb{R}^{k+1}}{\mathrm{argmin}} \left\| \mathcal{F}^{Q} \dot{\boldsymbol{\omega}} + \mathrm{Re}\left(\boldsymbol{C}\right) \right\|. \qquad (15)$$

It should be noted that the solution to Eq. (14) could alternatively be solved via pseudoinversion or even exact inversion if $\mathcal{F}^{Q}$ is invertible. The derivation of the global phase agnostic VarQITE ODE given in Eq. (14) is presented in Appendix D and details on the evaluation of the individual terms are given in Appendix G.

As before, the state gradients are likely to be inexact due to the variational approximation such that $\| |e_t\rangle \| > 0$ for the gradient error

$$|e_t\rangle := |\dot{\psi}_t^{\dot{\nu}}\rangle - \left(E_t^{\omega} - H\right) |\psi_t^{\omega}\rangle. \qquad (16)$$

Equation (16) again motivates an alternative VarQITE ODE formulation that aims at finding the parameter updates $\dot{\boldsymbol{\omega}}$ as

$$f_{\mathrm{err}}\left(\boldsymbol{\omega}\right) = \underset{\dot{\boldsymbol{\omega}} \in \mathbb{R}^{k+1}}{\mathrm{argmin}} \| |e_t\rangle \|_2^2, \qquad (17)$$

for

$$\| |e_t\rangle \|_2^2 = \mathrm{Var}(H)_{\psi_t^{\omega}} + \langle \dot{\psi}_t^{\omega} | \dot{\psi}_t^{\omega} \rangle - \langle \dot{\psi}_t^{\omega} | \psi_t^{\omega} \rangle \langle \psi_t^{\omega} | \dot{\psi}_t^{\omega} \rangle$$
$$+ 2\mathrm{Re}\left(\langle \dot{\psi}_t^{\omega} | H | \psi_t^{\omega} \rangle\right), \qquad (18)$$

using that

$$2\mathrm{Re}\left(\langle \psi_t^{\omega} | \dot{\psi}_t^{\omega} \rangle\right) = \frac{\partial \langle \psi_t^{\omega} | \psi_t^{\omega} \rangle}{\partial t} = 0. \qquad (19)$$

Since the time dependence of $|\psi_t^{\omega}\rangle$ is encoded in the parameters $\boldsymbol{\omega}$, we can rewrite Eq. (18)

$$\| |e_t\rangle \|_2^2 = \mathrm{Var}(H)_{\psi_t^{\omega}} + \sum_{i,j} \dot{\omega}_i \dot{\omega}_j \mathcal{F}_{ij}^{Q} + 2 \sum_i \dot{\omega}_i \mathrm{Re}(C_i),$$

where we employ the fact that

$$\mathrm{Re}\left(\langle \dot{\psi}_t^{\omega} | H | \psi_t^{\omega} \rangle\right) = \sum_i \dot{\omega}_i \mathrm{Re}(C_i), \qquad (20)$$

as well as Eq. (11). The efficient evaluation of $\| |e_t\rangle \|_2^2$ employs the techniques presented in Appendix G.

III. ERROR BOUNDS

In this section, we prove global phase agnostic error bounds for VarQTE. Let $|\psi_t^{\omega}\rangle$ be the state prepared by the variational algorithm at time t and denote the ideal target state by $|\psi_t^*\rangle$. To formalize a meaningful error bound, we want to use a metric, which describes the distance between two quantum states in a global phase agnostic way. For clarification, we shall consider the example of the distance between $|\psi\rangle$ and $-|\psi\rangle$. The distance of these states with respect to the ℓ_2-norm is 2 although the states are physically equivalent. A popular distance measure that is invariant to changes in the global phases is the fidelity [26] given by $|\langle \psi_t^{\omega} | \psi_t^* \rangle|^2$. This is a desired property for a meaningful quantum state distance measure. Although the fidelity itself does not correspond to a metric, it may be used to define the Bures metric [27], i.e.,

$$B\left(|\psi_t^{\omega}\rangle, |\psi_t^*\rangle\right) =$$
$$\sqrt{\langle \psi_t^{\omega} | \psi_t^{\omega} \rangle + \langle \psi_t^* | \psi_t^* \rangle - 2|\langle \psi_t^{\omega} | \psi_t^* \rangle|}, \qquad (21)$$

where the states $|\psi_t^{\omega}\rangle$ and $|\psi_t^*\rangle$ are not necessarily normalized. It should be noted that we use the simplified notation $B\left(|\psi_t^{\omega}\rangle, |\psi_t^*\rangle\right) := B\left(|\psi_t^{\omega}\rangle \langle \psi_t^{\omega}|, |\psi_t^*\rangle \langle \psi_t^*|\right)$.

Our goal is, now, to prove a bound of the form

$$B\left(|\psi_t^{\omega}\rangle, |\psi_t^*\rangle\right) \le \epsilon_t, \qquad (22)$$

for an error term ϵ_t that can be evaluated efficiently in practice. Interestingly, the error bounds with respect to the Bures metric are a direct consequence of the phase agnostic ODE formulation of VarQTE presented in the previous section. The aforementioned relation of the Bures metric to the fidelity

$$|\langle \psi_t^{\omega} | \psi_t^* \rangle| \ge 1 - \frac{\epsilon_t^2}{2}, \qquad (23)$$

implies that the relevant range of ϵ_t is $\epsilon_t \in \left[0, \sqrt{2}\right]$ for normalized $|\psi_t^{\omega}\rangle$ and $|\psi_t^*\rangle$. If the error bound estimate lies outside of this interval, then the fidelity and error can be clipped to 0 and $\sqrt{2}$, respectively.

A. Variational quantum real-time evolution

In Ref. [19] the authors derive an error bound for a VarQRTE formulation that does not include the global phase

compensating terms. Due to the global phase-dependent nature of the VarQRTE ODE, the resulting error bound presents an upper bound to the ℓ_2-error. We, now, align the theory with the global phase-independent formulation of VarQRTE and derive a corresponding error bound for the Bures metric, which helps to avoid that a physically irrelevant mismatch in the global phase influences the bound. The proof is given in Appendix E and a comparison between ℓ_2-norm and Bures metric error bound is given in Appendix IV D.

Theorem 1.—For $T > 0$ and $\epsilon_0 = 0$, let $|\psi_T^*\rangle$ be the exact solution to Eq. (13) and $|\psi_T^\omega\rangle$ correspond to the VarQRTE approximation. Then

$$B\left(|\psi_T^*\rangle, |\psi_T^\omega\rangle\right) \leq \epsilon_T := \int_0^T \||e_t\rangle\|_2 \, \mathrm{d}t \qquad (24)$$

for

$$\||e_t\rangle\|_2^2 = \mathrm{Var}(H)_{\psi_t^\omega} + \sum_{i,j} \dot{\omega}_i \dot{\omega}_j \, \mathcal{F}_{ij}^Q$$
$$- 2 \sum_i \dot{\omega}_i \, \mathrm{Im}\left(C_i - \frac{\partial \langle\psi_t^\omega|}{\partial \omega_i} |\psi_t^\omega\rangle E_t^\omega\right). \quad (25)$$

It should be noted that the error bound is compatible with practical VarQRTE implementations, which use, e.g., regularized least-squares methods or pseudoinversion methods to solve the system of linear equations from Eq. (4). Doing the same derivation but dropping the terms in the VarQRTE ODE that compensate for potential global phase changes, i.e., $\mathrm{Re}\left(\partial \langle\psi_t^\omega|/\partial\omega_i |\psi_t^\omega\rangle\langle\psi_t^\omega| \partial |\psi_t^\omega\rangle/\partial\omega_j\right)$ from $\mathcal{F}_{ij}^Q$ and $\partial \langle\psi_t^\omega|/\partial\omega_i |\psi_t^\omega\rangle E_t^\omega$, leads to error bounds for the ℓ_2-norm ϵ^{PD} [19]—see Appendix C for further details on the phase agnostic definition of VarQRTE.

B. Variational quantum imaginary-time evolution

This section introduces an upper bound to the Bures metric between the target state $|\psi_t^*\rangle$ given by Eq. (12) and $|\psi_t^\omega\rangle$ prepared with VarQITE. The proof is given in Appendix F.

Theorem 2.—For $T > 0$ and $\epsilon_0 = 0$, let $|\psi_T^*\rangle$ be the exact solution to Eq. (13) and $|\psi_T^\omega\rangle$ be the simulation implemented using VarQITE. Then

$$B\left(|\psi_T^*\rangle, |\psi_T^\omega\rangle\right) \leq \epsilon_T := \int_0^T \||e_t\rangle\|_2 \, \mathrm{d}t, \qquad (26)$$

for

$$\||e_t\rangle\|_2^2 = \mathrm{Var}(H)_{\psi_t^\omega} + \sum_{i,j} \dot{\omega}_i \dot{\omega}_j \, \mathcal{F}_{ij}^Q$$
$$+ 2 \sum_i \dot{\omega}_i \, \mathrm{Re}(C_i). \qquad (27)$$

This error bound is also independent of a potential physically irrelevant global phase mismatch between prepared and target state. Equivalently to VarQRTE, dropping the term in the VarQITE ODE that compensates for potential global phase changes, i.e., $\mathrm{Re}\left(\partial \langle\psi_t^\omega|/\partial\omega_i |\psi_t^\omega\rangle\langle\psi_t^\omega| \partial |\psi_t^\omega\rangle/\partial\omega_j\right)$ in $\mathcal{F}_{ij}^Q$, leads to error bounds for the ℓ_2-norm ϵ^{PD}—see Appendix D for further details on the global phase agnostic definition of VarQITE. Furthermore, the bound is compatible with implementations, which use numerical techniques to solve the system of linear equations (SLEs) given in Eq. (14).

IV. SIMULATION RESULTS

In this, we demonstrate the efficiency of the error bounds derived in Sec. III, as well as the impact of methodological choices such as the type of ODE solver and present an example that illustrates the significance of phase agnostic VarQITE error bounds. Unless otherwise stated, the experiments prepare $|\psi_t^\omega\rangle$ with an ansatz as shown in Fig. 2, adjusted to the number of qubits n given by the respective Hamiltonian:

(i) An illustrative example is considered with

$$H_{\mathrm{illustrative}} = Z \otimes X + X \otimes Z + 3Z \otimes Z. \qquad (28)$$

Hereby, the evolution time is $T = 1$ and the initial parameters are chosen such that all parameters are set to 0 except for the parameters of the last layer of RY rotations which are chosen to be $\pi/2$. This gives $|\psi_0\rangle = |++\rangle$.

(ii) The well-studied Ising model with a transverse magnetic field on an open chain is investigated, see, e.g., Ref. [29], i.e.,

$$H_{\mathrm{Ising}} = -J\left(\sum_{i,j} Z_i \otimes Z_j + g \sum_j X_j\right), \qquad (29)$$

where $J = -1/2$ and $g = -1/2$. While the following section includes examples with three qubits, additional results with ten qubits are presented in Appendix H. The evolution time is again set to $T = 1$ and the initial parameters are all 0 except for the parameters of the last layer of RZ gates, which are chosen at random in $(0, \pi/2]$ such that $|\psi_0\rangle = e^{-i\gamma}|000\rangle$ with $\gamma \in \mathbb{R}$. Notably, we avoid the initial state $|\psi_0\rangle = |000\rangle$ to circumvent getting stuck in a local minima.

(iii) The two qubit hydrogen molecule approximation given in Ref. [6] is studied, with

$$\begin{aligned} H_{\mathrm{hydrogen}} = {} & 0.2252\, I \otimes I + 0.5716\, Z \otimes Z \\ & + 0.3435\, I \otimes Z - 0.4347\, Z \otimes I \\ & + 0.0910\, Y \otimes Y + 0.0910\, X \otimes X. \end{aligned} \qquad (30)$$
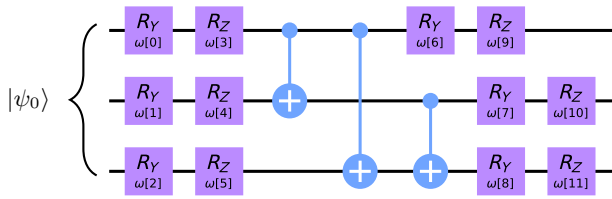
FIG. 2. This quantum circuit corresponds to the *EfficientSU2* ansatz in Qiskit's [28] circuit library and is chosen as ansatz for the experiments presented in this work. It consists of layers of *RY* and *RZ* rotations and a *CX* entanglement block which is chosen according to the *full* layout. The number of repetitions is set to 1.

Again, the evolution time is set to $T = 1$ and the initial parameters are chosen such that the initial state is $|\psi_0\rangle = |++\rangle$, i.e., all parameters are 0 except for the last layer of *RY* rotations, which are given as $\pi/2$.

A. Methods

To ensure a stable VarQTE implementation, it is vital to choose the appropriate settings. In the following section, we are going to discuss a variety of methodological choices that are relevant for the simulation performance of VarQTE.

The ODE underlying VarQTE is solved using numerical integration. Let $|\psi_t^*\rangle$ denote the target state, $|\psi_t^\omega\rangle$ the prepared state, and $|\psi_t'\rangle$ the state that we would prepare if we could take infinitesimally small time steps and, thus, integrate the ODE exactly. The error bounds derived in Sec. III capture the errors solely induced by the variational method, i.e.,

$$B\left(|\psi_t^*\rangle, |\psi_t'\rangle\right) \leq \epsilon_t. \tag{31}$$

The triangle inequality gives

$$B\left(|\psi_t^*\rangle, |\psi_t^\omega\rangle\right) \leq B\left(|\psi_t^*\rangle, |\psi_t'\rangle\right) + B\left(|\psi_t'\rangle, |\psi_t^\omega\rangle\right). \tag{32}$$

The error term induced by the numerical integration $B(|\psi_t'\rangle, |\psi_t^\omega\rangle)$ is generally unknown. In order for the error bounds from Sec. III to hold $B(|\psi_t'\rangle, |\psi_t^\omega\rangle) \ll 1$ such that

$$B\left(|\psi_t^*\rangle, |\psi_t^\omega\rangle\right) \approx B\left(|\psi_t^*\rangle, |\psi_t'\rangle\right) \leq \epsilon_t. \tag{33}$$

ODE solvers, such as the *forward Euler* method, which operate with a fixed step size may induce large errors in the numerical simulations if the time steps are not chosen sufficiently small. The forward Euler method evaluates the gradient $\dot{\omega}_t$ and propagates the underlying variable for n_T time steps according to a predefined step size, i.e.,

$$\omega_T = \omega_0 + \sum_{k=0}^{n_T} \delta_t \dot{\omega}_{t_k}, \tag{34}$$

with $t_{n_T} = T$ and the step size $\delta_t = t_{k+1} - t_k$. In contrast, *Runge-Kutta* methods evaluate additional supporting

points and compute a parameter update using an average of these points, thereby, truncating the local update error. Combining two Runge-Kutta methods of different order but using the same supporting points allows definition of efficient adaptive step-size ODE solvers, which ensure that the local step-by-step error is small and, thus, that the dominant part of the error is coming from the variational approximation. The results in Sec. IV illustrate this aspect on the example of the forward Euler method [30] with fixed step size and an explicit Runge-Kutta method of order 5(4) (RK54) method from SciPy [31] that uses additional interpolation points as well as an adaptive step size to minimize the step-by-step integration errors. We refer the interested reader to an introductory book on numerical ODE solvers such as Ref. [30].

The SLE underlying McLachlan's variational principle, given in Eqs. (4) and (14), are prone to being ill conditioned and may, thus, only be solvable approximately with a numerical technique such as regularized least squares or pseudoinversion. In the following, we shall refer to the ODE definition based on f_{res} as *residual ODE*. The ODE definition f_{err}—which shall be referred to as *gradient error ODE*—is analytically equivalent to solving f_{res}. However, the simulation results in Sec. IV show that the numerical behavior differs. In fact, the experiments reveal that the gradient error ODE can often lead to better numerical stability. The simulations employ the SciPy COBYLA optimizer [31] to find $\dot{\omega}$ in f_{err} where the initial point is chosen as the numerical solution to the SLE given in Eqs. (4) and (14), respectively.

In practice, we jointly evolve the state parameters and the error bounds. More explicitly, we extend the ODE to

$$\begin{pmatrix} \dot{\omega}_t \\ \dot{\epsilon}_t \end{pmatrix} = \tilde{f}(\omega_t, \epsilon_t), \tag{35}$$

with ω_0 being set, $\epsilon_0 = 0$ by assumption, and

$$\tilde{f}(\omega_t, \epsilon_t) = \begin{pmatrix} f(\omega_t) \\ \||e_t\rangle\|_2 \end{pmatrix}, \tag{36}$$

with $\||e_t\rangle\|_2$ from Eqs. (25) and (27) for the real and imaginary case, respectively. Furthermore, $f(\omega_t)$ is either chosen as $f_{\text{res}}(\omega_t)$ or $f_{\text{err}}(\omega_t)$. This formulation has the advantage that the error bound directly reflects the propagation of the evolution and that adaptive step-size ODE solvers also consider the changes in the error bounds.

B. Variational quantum real-time evolution

In the following, we present a set of numerical experiments and investigate the error bounds for VarQRTE with a particular focus on the comparison of different ODE formulations and solvers.

Firstly, we apply the forward Euler method with 100 time steps as well as an adaptive step-size RK54 ODE
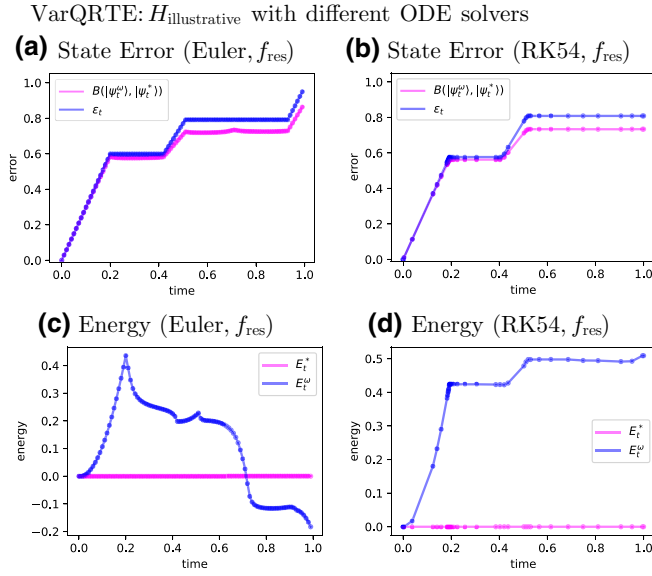
VarQRTE: $H_{\text{illustrative}}$ with different ODE solvers

(a) State Error (Euler, f_{res}) **(b)** State Error (RK54, f_{res})

(c) Energy (Euler, f_{res}) **(d)** Energy (RK54, f_{res})

FIG. 3. VarQRTE for $|\psi_0\rangle = |++\rangle$, $H_{\text{illustrative}}$, and $T = 1$ with the residual ODE. (a),(c) Employ forward Euler. (b),(d) Use RK54. (a),(b) illustrate the error bounds ϵ_t and the actual Bures metric between $|\psi_t^*\rangle$ and $|\psi_t^\omega\rangle$. (c),(d) show the corresponding energies.

VarQRTE: H_{Ising} with different ODE definitions

(a) State Error (RK54, f_{res}) **(b)** State Error (RK54, f_{err})

(c) Energy (RK54, f_{res}) **(d)** Energy (RK54, f_{err})

FIG. 4. VarQRTE for $|\psi_0\rangle = e^{-i\alpha}|000\rangle$, H_{Ising}, and $T = 1$ with RK54. (a),(c) are based on the residual ODE. (b),(d) use the gradient error ODE. (a),(b) illustrate the error bounds ϵ_t and the actual Bures metric. (c),(d) show the energies corresponding to prepared and target state.

solver to the illustrative example using the residual ODE. The parameter propagation given by f_{res} is solved using a least-squares solver provided by NumPy [32] with a cut-off ratio for small singular values of 0.001. The results shown in Fig. 3 illustrate that the error bounds are very tight and, thus, relevant for practical accuracy estimations. Furthermore, one can see that RK54 achieves a state preparation with less error compared to forward Euler—which is reflected in the error bounds—as well as smaller fluctuations in the system energy while using significantly less time steps. The plateaus are due to exact local gradients, i.e., $\| |e_t\rangle \|_2 = 0$. Furthermore, we would like to point out that the energy should actually be preserved for a real-time evolution under a time-independent Hamiltonian but McLachlan's variational principle does not guarantee energy preservation.

Next, we compare the impact of f_{res} compared to f_{err} on the example of an Ising model using RK54. Here, f_{res} and f_{err} are solved with a least-squares solver provided by NumPy [32] and an additional regularization on the Fubini-Study metric. More explicitly, we use $\tilde{\mathcal{F}} = \mathcal{F} + \gamma \mathbb{1}$ for a small γ. The initial points for the optimization of the gradient error ODE are chosen as the solution to the respective SLE at time t. Figure 4 presents the Bures metrics, as well as the respective bounds for the prepared $|\psi_t^\omega\rangle$ and the target state $|\psi_t^*\rangle$. The errors show that the gradient error ODE leads to smaller errors than the residual ODE. Furthermore, it can be seen that also the system energy changes less for the former. Furthermore, Appendix H shows error bound results for an Ising model
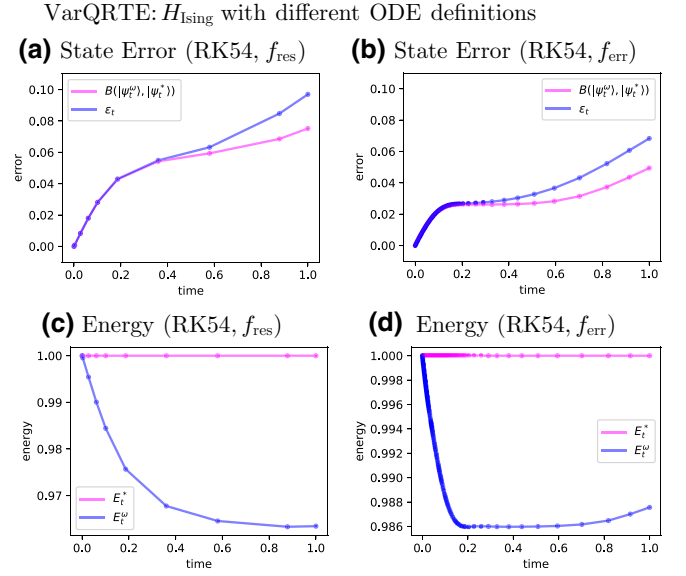
with ten qubits. These experiments highlight the potential of the error bounds to be applicable for systems with larger dimensions.

Lastly, the error bounds for the hydrogen Hamiltonian from Eq. (30) are compared to the residual and gradient error ODE as well as forward Euler and RK54 ODE solvers. In this case, f_{res} and f_{err} are solved using ridge regression, also known as Tikhonov regularization, from SciKit [33]. This method is also used to compute the initial values for the gradient error ODE formulation. The results are presented in Fig. 5. Notably, the experiment that uses RK54 and the gradient error ODE leads to the best results, i.e., the smallest state error as well as error bound. In general, one can see that the gradient error ODE achieves better errors compared to the residual ODE, the error seems to saturate for the former while it keeps increasing with the latter. Furthermore, RK54 improves the errors, as well as the error bounds for both ODE definitions while using significantly less time steps. We would like to point out that the setting, which gives the smallest error ϵ_t, does not necessarily lead to the smallest discrepancy between E_t^ω and E_t^*, as can be seen when comparing the RK54 results.

To sum this up, the numerical results reveal that the error bounds represent good estimates for the actual errors. The experiments indicate further that an adaptive step-size ODE solver such as RK54 significantly improves the simulation results while reducing the computational costs. Moreover, it was shown that replacing the residual ODE by the gradient error ODE has also a positive influence
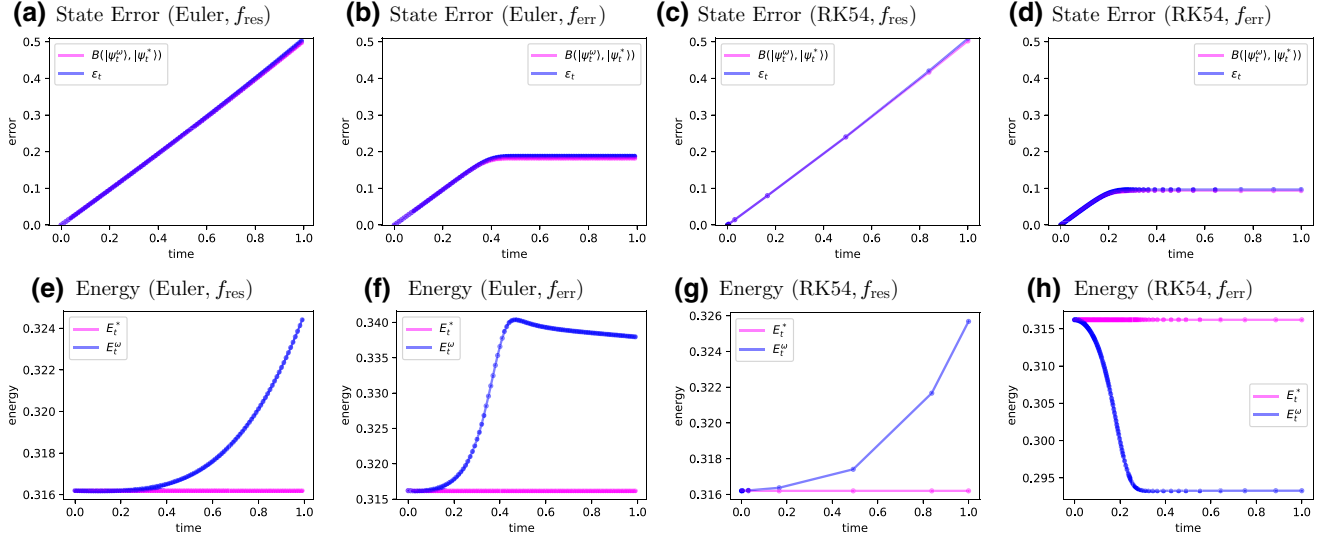
FIG. 5.   VarQRTE for $|\psi_0\rangle = |++\rangle$, H_{hydrogen} and $T = 1$. (a),(b),(e),(f) employ a forward Euler solver. (c),(d),(g),(h) use an RK54 ODE solver. (a),(c),(e),(g) use the residual ODE. (b),(d),(f),(h) rely on the gradient error ODE. (a),(b),(c),(d) illustrate the error bounds ϵ_t and the true Bures metric. (e),(f),(g),(h) show the respective energies E_t^ω and E_t^*.

on the simulation accuracy. Lastly, the results reveal that the lack of energy conservation in McLachlan's variational principle can lead to significant energy fluctuations.

C. Variational quantum imaginary-time evolution

Next, we investigate the practical behavior of the error bounds for VarQITE. First, the outcomes using the residual ODE with forward Euler as well as RK54 are compared for $H_{\text{illustrative}}$. For all of the following experiments, f_{res} and f_{err} are evaluated with ridge regression. The results shown in Fig. 6 provide an example of the potentially insufficient numerical integration accuracy of forward Euler. More explicitly, the integration error outweighs the algorithmic error and, hence, the error bounds are at first lower than the actual error. The application of RK54 in comparison reduces the error in the integration. The fidelity plots translate the error bound into a physically easy to interpret distance metric.

Next, the performance of the residual and gradient error ODE formulation is compared on the example of H_{Ising} using RK54 for an evolution over time $T = 5$ using a least-squares solver provided by NumPy [32] with a cutoff ratio for small singular values of 0.001. Figure 7 illustrates the sensitivity of the variational errors to the underlying ODE formulation. More explicitly, the errors and corresponding bounds are more than twice as big for the VarQITE implementation based on f_{res} compared to the one based on f_{err}. The larger state error also manifests itself in a deviation of the system energy. Appendix H shows progress towards a study of error bounds for larger system dimensions with a ten-qubit Ising model.

In all previous examples the gradient error ODE formulation leads to better performance. Next, we are going to investigate an example for H_{hydrogen} where the residual ODE turns out to be the preferable method. We tested a variety of settings and found that while the residual ODE was leading to reasonable results in most cases, the
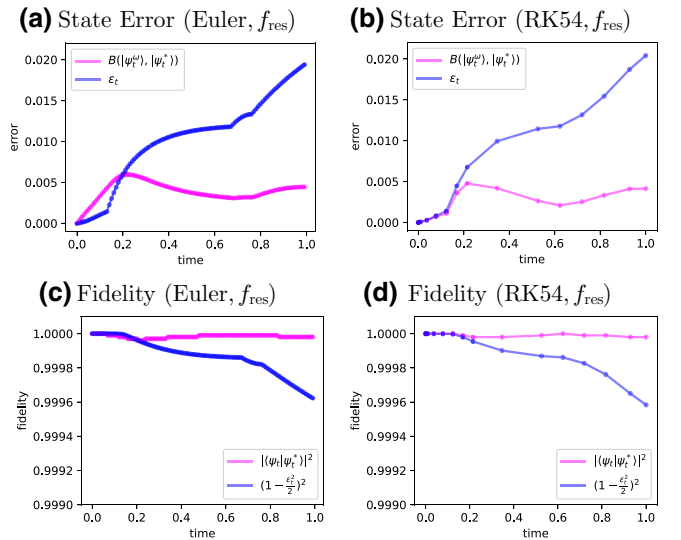

FIG. 6.   VarQITE for $|\psi_0\rangle = |++\rangle$, $H_{\text{illustrative}}$ and $T = 1$ with the residual ODE (a),(c) are computed using forward Euler. (b),(d) Employ RK54. (a),(b) illustrate the error bound ϵ_t and the true Bures metric. Furthermore, (c),(d) show the true fidelities and fidelity bounds.
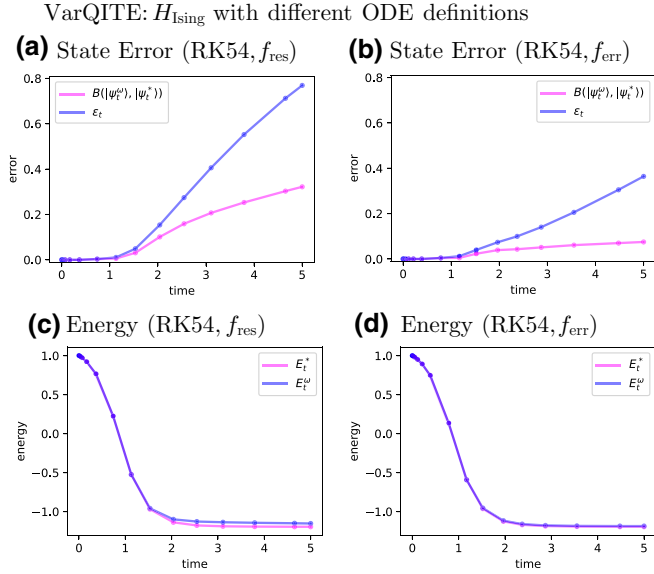
FIG. 7. VarQITE for $|\psi_0\rangle = e^{-i\gamma}|000\rangle$, H_{Ising}, and $T = 5$ with RK54. (a),(c) employ the residual ODE. (b),(d) use the gradient error ODE. (a),(b) illustrate the error bound ϵ_t, as well as the actual Bures metric. (c),(d) present the corresponding energy evolution.

gradient ODE often leads to spiky gradient errors and, eventually, to large state errors. One set of results is visualized in Fig. 8. It is clearly illustrated that the residual ODE formulation leads to a significantly better evolution with errors and error bounds that are on the order of 10^{-3} compared to a maximal error approximately equal to 0.56 around $T = 5$ and a bound converging to $\sqrt{2}$ for f_{err}. Interestingly, in the latter case the energy with respect to the prepared state E_t^ω first strongly deviates from E_t^* but finally reaches similar values again. This indicates that VarQITE provides a promising method for ground-state search where the evolution does not necessarily need to be followed perfectly at all times. The presented results were computed using again a regularization on the Fubini-Study metric: $\tilde{\mathcal{F}} = \mathcal{F} + \gamma \mathbb{1}$ for a small γ.

D. Global phase dependence

We employ an illustrative example to compare the error bound for VarQRTE derived in this work to the error bound presented in Ref. [19] and, thereby, highlight the significance of phase agnostic metrics. Given the Hamiltonian $H = Z$, we consider the evolution of the initial state $|\psi_0\rangle = |1\rangle$ by e^{-iHT} for $T = 1$. It should be noted that this time evolution solely affects the global phase of $|\psi_0\rangle$ that, as discussed in the main text, is physically irrelevant. We run VarQRTE with two exemplary ansätze

(1) $|\psi_t^\omega\rangle = RY(\omega_0)|1\rangle$, which does not enable the representation of a global phase change, and
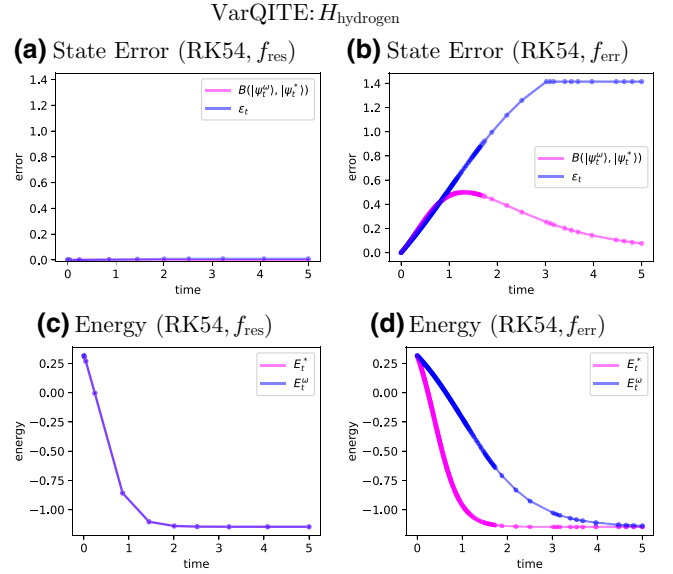
(2) $|\psi_t^\omega\rangle = RY(\omega_1)RZ(\omega_0)|1\rangle$, which does enable the representation of a global phase change.

Figure 9 shows the error bounds for VarQRTE using the phase agnostic (phase-dependent) McLachlan's variational

FIG. 8. VarQITE for $|\psi_0\rangle = |++\rangle$, H_{hydrogen}, and $T = 5$. All plots are based on RK54 and either the (a),(c) residual or the (b),(d) gradient error ODE. (a),(b) illustrate the error bound ϵ_t, as well as the actual Bures metric. Furthermore, (c),(d) present the system energy E_t^ω corresponding to the prepared state and the energy E_t^* corresponding to the target state.
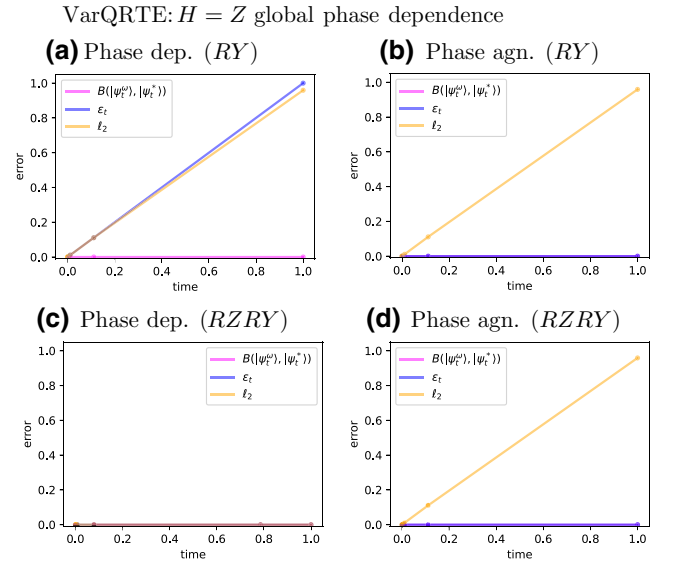

FIG. 9. VarQRTE error bounds for $|\psi_0\rangle = |1\rangle$, $H = Z$, and $T = 1$ with RK54. (a),(c) are based on the phase-dependent definition of the VarQRTE ODE and the error bound (b),(d) use the phase agnostic definition. (a),(b) employs ansatz 1. (c),(d) employs ansatz 2.
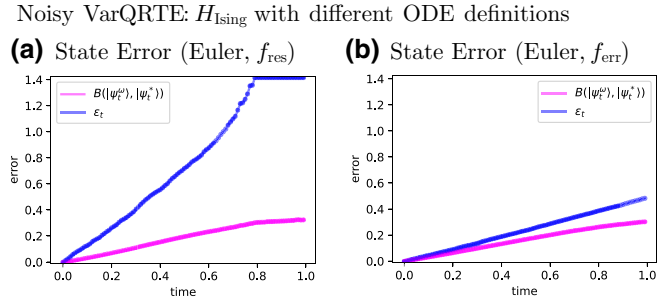
Noisy VarQRTE: H_{Ising} with different ODE definitions

FIG. 10. VarQRTE for $|\psi_0\rangle = e^{-i\alpha}|000\rangle$, H_{Ising}, and $T = 1$ with forward Euler. (a) is based on the residual ODE. (b) uses the gradient error ODE. Both illustrations show the error bounds ϵ_t and the actual Bures metric.

principle leading to an upper bound ϵ_t (ϵ_t^{PD}) for the Bures metric (ℓ_2-norm). The figures also present the exact errors. All experiments are run with an RK54 ODE solver using the residual ODE with all ansatz parameters being initially set to 0.

Given the *RY* ansatz, the ℓ_2-norm deviates significantly from the Bures metric. While the error bound for the phase-dependent formulation ϵ_t^{PD} leads to large values the phase agnostic bound ϵ_t directly reflects that the physics of the system do not change. The results further illustrate that the *RZRY* ansatz enables the mitigation of the above problem by training an additional parameter to match the global phase change induced by the evolution. The phase agnostic formulation can, thus, help to avoid the implementation of an additional gate and parameter—whose training may potentially induce errors—while capturing the physics of the problem.

E. Hardware simulation

The experiments presented so far are run with ideal simulations. However, it is of course also useful to understand how the error bounds would perform if the respective quantities would be evaluated with quantum hardware that is affected by physical noise. As a study of the robustness of our bounds to hardware noise, we test a VarQRTE experiment for H_{Ising} described in Sec. IV with a noisy simulation for runtime $T = 1$. More explicitly, we employ a *density-matrix simulator* with a noise model that represents the physical errors of the *IBM Quantum Auckland* backend to evaluate the system variance $\text{Var}(H)_{\psi_t^\omega}$, the QFI $\mathcal{F}_{ij}^Q$, and the quantity $\text{Im}\left(C_i - \partial \langle \psi_t^\omega|/\partial \omega_i |\psi_t^\omega\rangle E_t^\omega\right)$ given in Eq. (4), respectively, Eq. (9). Each evaluation is based on 10 000 samples that are measured from the quantum circuits. These quantities are then used to evaluate the ODE function to propagate the parameters and to compute the noisy error bound ϵ_T. This error-bound evaluation is compared to the Bures metric between the target state and the state underlying our noisy simulation given as a density

matrix. The results are presented in Fig. 10 for the residual as well as the gradient error ODE formulation. While the residual ODE formulation converges to the maximal value of $\sqrt{2}$ and, hence, does not enable the capture of the true Bures metric, the dual formulation shows more robustness against the simulated noise, i.e., the final error bound is 0.4823 while the actual error is 0.3018.

V. CONCLUSION AND OUTLOOK

This work presents *a posteriori* error bounds for the Bures metric between a state prepared with VarQTE and the respective unknown target state resulting from exact QTE. These bounds enable users to quantify the accuracy of their quantum time-evolution simulation and potentially adapt their simulation setting if necessary.

The presented *a posteriori*, algorithmic error bounds for VarQTE lower bound existing error bounds [17,19]. Furthermore, the bounds are particularly simple to evaluate, i.e., the additional resource overhead is limited to the evaluation of the energy variance.

We show that the error bounds and VarQTE itself are strongly dependent on the numerical integration method. An ODE solver, which applies an adaptive step-size scheme, can increase the numerical stability and accuracy significantly. Furthermore, using an ODE formulation, which is based on the minimization of the local gradient error $\| |e_t\rangle \|_2$ often helps to reduce the simulation errors. The performance of the algorithm, the error bounds, related state fidelities, and system energies are demonstrated on numerical examples.

An open question for future research would be the investigation of the behavior of the error bounds at critical points, such as phase transitions. This study could give us useful insights into the limits and potentials of the QTE simulation technique. Furthermore, it would be of interest to conduct an enhanced study about the robustness of the error bounds under realistic quantum hardware conditions.

The code can be made available upon reasonable request. All quantities required to compute the presented error bounds can be evaluated with the tools provided by Qiskit's gradient framework [28,34].

APPENDIX A: RESOURCE OVERHEAD

This section analyzes the additional computational resources required to evaluate the error bound ϵ_T for VarQTE simulations given shot-based estimations.

The resources required to compute ϵ_T eventually depend on the estimation of

$$\||e_t\rangle\|_2^2 = \mathrm{Var}(H)_{\psi_t^\omega} + \dot{\boldsymbol{\omega}}^T \mathcal{F}^Q \dot{\boldsymbol{\omega}} + 2\dot{\boldsymbol{\omega}}^T \mathbf{c}, \qquad (A1)$$

in each time step of the numerical ODE integration with $\mathbf{c}$ referring to $\mathbf{c}_R := -\mathrm{Im}\left(\mathbf{C} - (\nabla_\omega \langle \psi_t^\omega |)|\psi_t^\omega\rangle E_t^\omega\right)$ for the VarQRTE and $\mathbf{c}_I := \mathrm{Re}(\mathbf{C})$ for the VarQITE case. Since $\mathbf{c}$ and $\mathcal{F}^Q$ are already part of the VarQTE calculations, the resource overhead solely depends on $\mathrm{Var}(H)_{\psi_t^\omega}$. To simplify the notation we will drop the state subscript in the following.

Assuming that the system Hamiltonian is given as a weighted sum of Pauli operators $H = \sum_{i=0}^{s-1} \alpha_i h_i$ with $h_i = \bigotimes_{j=0}^{n-1} \sigma_{ij}$ for $\sigma_{ij} \in \{\mathbb{1}, X, Y, Z\}$ and $\alpha_i \in [-a, a]$, we can bound

$$\begin{aligned}
\mathrm{Var}\,&[\mathrm{Var}(H)] \\
&= \mathrm{Var}\left[H^2\right] + \mathrm{Var}\left[H|\psi_t^\omega\rangle\langle\psi_t^\omega|H\right] \\
&\quad - \mathrm{Cov}\left[H^2, H|\psi_t^\omega\rangle\langle\psi_t^\omega|H\right] \\
&= \langle\psi_t^\omega|H^4|\psi_t^\omega\rangle - \langle\psi_t^\omega|H^3|\psi_t^\omega\rangle E - \mathrm{Var}(H)^2 \\
&\leq \langle\psi_t^\omega|H^4 - EH^3|\psi_t^\omega\rangle \\
&\leq \left|\langle\psi_t^\omega|H^4 - EH^3|\psi_t^\omega\rangle\right| \\
&\leq \lambda_{\max}\left[H^4 - EH^3\right] \\
&\leq \left\|H^4 - EH^3\right\|_\infty \\
&\leq \left\|H^4\right\|_\infty + |E|\left\|H^3\right\|_\infty \\
&= \|H\|_\infty^4 + |E|\|H\|_\infty^3 \\
&\leq (sa)^4 + |E|(sa)^3, \qquad (A2)
\end{aligned}$$

where Cov denotes the covariance, $\lambda_{\max}[X]$ corresponds to the maximum eigenvalue of X, and $\|X\|_\infty$ represents the infinity norm. The third to last line is based on the triangle inequality and the second to last line employs a property of the infinity norm. Finally, the last line uses that

$$\|H\|_\infty = \left\|\sum_{i=0}^{s-1} \alpha_i h_i\right\|_\infty \leq \sum_{i=0}^{s-1} |\alpha_i|\, \|h_i\|_\infty \leq sa. \qquad (A3)$$

Now, the error in the N-shot estimate $\hat{V}$ of $\mathrm{Var}(H)$ behaves as

$$P\left(\left|\mathrm{Var}(H) - \hat{V}\right| \geq \delta_{\hat{V}}\right) := p_{\hat{V}} \leq \frac{\mathrm{Var}\,[\mathrm{Var}(H)]}{\delta_{\hat{V}}^2 N}. \qquad (A4)$$

It follows that $\delta_{\hat{V}}$ is bounded by

$$\delta_{\hat{V}} \leq \sqrt{\frac{(sa)^4 + |E|(sa)^3}{p_{\hat{V}} N}}. \qquad (A5)$$

Given τ time steps in the numerical ODE integration, N, thus, scales with $\mathcal{O}\left(\tau s^4/\delta_{\hat{V}}^2\right)$.

The number of shots $\tilde{N}$ needed to limit the shot noise in τ time steps of the variational state propagation of $|\psi_t^\omega\rangle$ to an error $\delta_{\psi_t^\omega}$ scales with $\mathcal{O}\left(T^2 k^3 \lambda_{\max}^2[H]/\tau \delta_{\psi_t^\omega}^2\right)$. In the setting considered here, $|\lambda_{\max}[H]| \leq sa$, which leads to a scaling of the form $\mathcal{O}\left(T^2 k^3 s^2/\tau \delta_{\psi_t^\omega}^2\right)$. While the resource overhead induced by the error-bound evaluation is quadratically more expensive in the number Pauli terms in the Hamiltonian, it is also independent of the number parameters k. Assuming that the number parameters k scales (as it often does) with $n \log(n)$, the scaling of N for the error bound does not exceed the scaling for $\tilde{N}$ with respect to the number qubits n if s scales at most with $\mathcal{O}\left((n \log(n))^{3/2}\right)$. Hence, the error-bound evaluation is not changing the overall complexity of the VarQTE algorithm under the described conditions.

APPENDIX B: INEQUALITY RELATIONS OF DISTANCE METRICS

This section presents a formal introduction to the metric inequalities illustrated in Fig. 1. If the states are normalized, then the Bures metric simplifies to

$$\begin{aligned}
B\left(|\psi_t^\omega\rangle, |\psi_t^*\rangle\right) &= \sqrt{2 - 2|\langle\psi_t^\omega|\psi_t^*\rangle|} \\
&= \min_{\phi \in [0, 2\pi]} \left\|e^{i\phi}|\psi_t^\omega\rangle - |\psi_t^*\rangle\right\|_2. \qquad (B1)
\end{aligned}$$

The last line highlights that the Bures metric can be interpreted as a global phase invariant ℓ_2-norm and, hence, $B\left(|\psi_t^\omega\rangle, |\psi_t^*\rangle\right) \leq \left\||\psi_t^\omega\rangle - |\psi_t^*\rangle\right\|_2$. The Bures metric is equivalent to the ℓ_2-norm if

(i) VarQTE does not induce a change in the global phase, or

(ii) $|\psi_t^\omega\rangle$ can represent a global phase change, e.g., with an additional phase gate [35].

However, one may not *a priori* know whether a global phase change is induced by the considered Hamiltonian and an additional phase gate can introduce additional noise as well as imprecision in the parameter propagation. Hence, the Bures metric offers an alternative to the ℓ_2-norm, which captures the properties of the systems while being agnostic to unphysical dependencies on global phases.
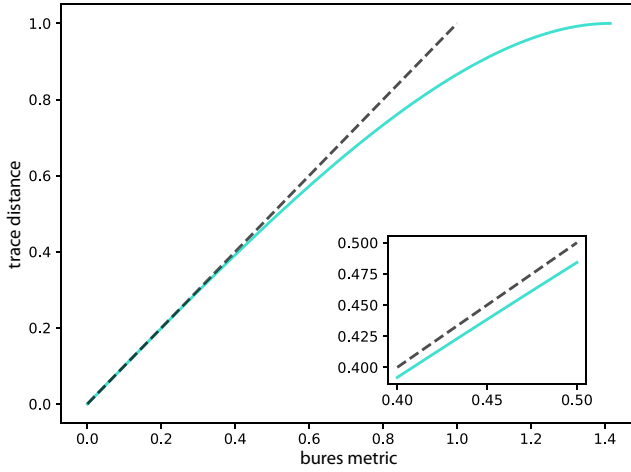
FIG. 11. The figure shows the trace distance as a function of the Bures metric (solid line) and, hence, the trajectory on which an upper bound to the trace distance based on ϵ would exist. The dashed diagonal illustrates the Bures metric itself until the maximum trace distance value 1 is reached.

Furthermore, the trace distance

$$D_{\mathrm{Tr}}\left(|\psi_t^\omega\rangle, |\psi_t^*\rangle\right) = \frac{1}{2}\left\| |\psi_t^\omega\rangle\langle\psi_t^\omega| - |\psi_t^*\rangle\langle\psi_t^*| \right\|, \quad \text{(B2)}$$

where we use the simplified notation $D_{\mathrm{Tr}}\left(|\psi_t^\omega\rangle, |\psi_t^*\rangle\right) := D_{\mathrm{Tr}}\left(|\psi_t^\omega\rangle\langle\psi_t^\omega|, |\psi_t^*\rangle\langle\psi_t^*|\right)$, can be defined via the fidelity if the underlying states are pure

$$D_{\mathrm{Tr}}\left(|\psi_t^\omega\rangle, |\psi_t^*\rangle\right) = \sqrt{1 - |\langle\psi_t^\omega|\psi_t^*\rangle|^2}. \quad \text{(B3)}$$

It follows that for pure states

$$D_{\mathrm{Tr}}\left(|\psi_t^\omega\rangle, |\psi_t^*\rangle\right) = \sqrt{1 - \left(1 - \frac{B\left(|\psi_t^\omega\rangle, |\psi_t^*\rangle\right)^2}{2}\right)^2}, \quad \text{(B4)}$$

and, hence, that $D_{\mathrm{Tr}}\left(|\psi_t^\omega\rangle, |\psi_t^*\rangle\right) \le B\left(|\psi_t^\omega\rangle, |\psi_t^*\rangle\right)$, where equality only holds if $|\psi_t^\omega\rangle = |\psi_t^*\rangle$. The relation is illustrated in Fig. 11.

APPENDIX C: GLOBAL PHASE AGNOSTIC VarQRTE

We are now going to derive the ODE given in Eq. 4. Consider the real-time evolution of a parameterized state with an explicit time-dependent global phase parameter ν, i.e., $|\psi_t^\nu\rangle = e^{-i\nu}|\psi_t^\omega\rangle$ for $\nu = \nu_t \in \mathbb{R}$, where $|\dot\psi^\nu\rangle = -i\dot\nu\, e^{-i\nu}|\psi_t^\omega\rangle + e^{-i\nu}|\dot\psi_t^\omega\rangle$. The Schrödinger equation with

respect to $|\psi_t^\nu\rangle$ reads

$$i|\dot\psi^\nu\rangle = H|\psi^\nu\rangle \quad \text{(C1)}$$

and can be rewritten as

$$i\, e^{-i\nu}|\dot\psi_t^\omega\rangle = (H - \dot\nu\mathbb{1})\, e^{-i\nu}|\psi_t^\omega\rangle. \quad \text{(C2)}$$

To simplify the notation, we shall from now on refer to $\dot\nu\mathbb{1}$ as $\dot\nu$. Division by $e^{-i\nu}$ gives

$$i|\dot\psi_t^\omega\rangle = (H - \dot\nu)|\psi_t^\omega\rangle. \quad \text{(C3)}$$

Applying McLachlan's variational principle [20] to Eq. (C3) leads to

$$\delta\left\| i|\dot\psi_t^\omega\rangle - (H - \dot\nu)|\psi_t^\omega\rangle \right\|_2 = 0, \quad \text{(C4)}$$

where $\|x\|_2 = \sqrt{\langle x, x\rangle}$. To find an explicit expression for $\dot\nu$, we evaluate the respective variational principle, i.e.,

$$\delta_{\dot\nu}\left\| i|\dot\psi_t^\omega\rangle - (H - \dot\nu)|\psi_t^\omega\rangle \right\|_2 = 0, \quad \text{(C5)}$$

which leads to

$$\dot\nu = E_t^\omega + \mathrm{Im}\left(\langle\dot\psi_t^\omega|\psi_t^\omega\rangle\right), \quad \text{(C6)}$$

where $E_t^\omega := \langle\psi_t^\omega|H|\psi_t^\omega\rangle$.

Finally, we can see that this formulation describes an evolution for $|\psi_t^\omega\rangle$, which simulates the existence of the global phase parameter ν without actually integrating or tracking $e^{-i\nu}$, i.e.,

$$i|\dot\psi_t^{\dot\nu}\rangle = H|\psi_t^\omega\rangle, \quad \text{(C7)}$$

where $|\dot\psi_t^{\dot\nu}\rangle := |\dot\psi_t^\omega\rangle - i(E_t^\omega + \mathrm{Im}(\langle\dot\psi_t^\omega|\psi_t^\omega\rangle))|\psi_t^\omega\rangle$ represents the effective state gradient. McLachlan's variational principle now implies

$$\delta\| i|\dot\psi_t^{\dot\nu}\rangle - H|\psi_t^\omega\rangle \|_2 = 0. \quad \text{(C8)}$$

Since $|\psi_t^\omega\rangle$ is given by a parameterized quantum circuit, solving Eq. (C8) with $|\dot\psi_t^\omega\rangle = \sum_i \dot\omega_i \frac{\partial|\psi_t^\omega\rangle}{\partial\omega_i}$ results in

$$\sum_{j=0}^k \mathrm{Re}\left(\frac{\partial\langle\psi_t^\omega|}{\partial\omega_i}\frac{\partial|\psi_t^\omega\rangle}{\partial\omega_j} - \frac{\partial\langle\psi_t^\omega|}{\partial\omega_i}|\psi_t^\omega\rangle\langle\psi_t^\omega|\frac{\partial|\psi_t^\omega\rangle}{\partial\omega_j}\right)\dot\omega_j$$

$$= \mathrm{Im}\left(\frac{\partial\langle\psi_t^\omega|}{\partial\omega_i}H|\psi_t^\omega\rangle - \frac{\partial\langle\psi_t^\omega|}{\partial\omega_i}|\psi_t^\omega\rangle E_t^\omega\right). \quad \text{(C9)}$$

APPENDIX D: GLOBAL PHASE AGNOSTIC VarQTE

Next, the derivation for the ODE given in Eq. (14) is presented. The normalized, Wick-rotated Schrödinger equation of an evolution of the state $|\psi_t^\nu\rangle = e^{-i\nu} |\psi_t^\omega\rangle$ reads

$$|\dot\psi^\nu\rangle = \left(E_t^\omega - H\right) |\psi^\nu\rangle, \tag{D1}$$

where

$$|\dot\psi^\nu\rangle = e^{-i\nu} |\dot\psi_t^\omega\rangle - i\dot\nu\, e^{-i\nu} |\psi_t^\omega\rangle. \tag{D2}$$

Thus,

$$e^{-i\nu} |\dot\psi_t^\omega\rangle = \left(E_t^\omega - H + i\dot\nu\right) e^{-i\nu} |\psi_t^\omega\rangle \tag{D3}$$

and division by $e^{-i\nu}$ leads to

$$|\dot\psi_t^\omega\rangle = \left(E_t^\omega - H + i\dot\nu\right) |\psi_t^\omega\rangle. \tag{D4}$$

Application of McLachlan's variational principle gives

$$\delta \left\| |\dot\psi_t^\omega\rangle - \left(E_t^\omega - H + i\dot\nu\right) |\psi_t^\omega\rangle \right\|_2 = 0. \tag{D5}$$

Next, we evaluate the variational principle with respect to $\dot\nu$

$$\delta_{\dot\nu} \left\| |\dot\psi_t^\omega\rangle - \left(E_t^\omega - H + i\dot\nu\right) |\psi_t^\omega\rangle \right\|_2 = 0 \tag{D6}$$

and find that $\dot\nu = -\text{Im}(\langle\dot\psi_t^\omega|\psi_t^\omega\rangle)$. Now,

$$|\dot\psi_t^{\dot\nu}\rangle = \left(E_t^\omega - H\right) |\psi_t^\omega\rangle \tag{D7}$$

simulates a global phase degree of freedom ν without actual implementation of $e^{-i\nu}$ and has the effective state gradient

$$|\dot\psi_t^{\dot\nu}\rangle := |\dot\psi_t^\omega\rangle + i\text{Im}(\langle\dot\psi_t^\omega|\psi_t^\omega\rangle) |\psi_t^\omega\rangle. \tag{D8}$$

Rewriting the variational principle accordingly gives

$$\delta \left\| |\dot\psi_t^{\dot\nu}\rangle - \left(E_t^\omega - H\right) |\psi_t^\omega\rangle \right\|_2 = 0. \tag{D9}$$

Since the time dependence of $|\psi_t^\omega\rangle$ is encoded in the parameters $\boldsymbol\omega$, Eq. (D9) leads to the following system of linear equations:

$$\sum_{j=0}^{k} \text{Re}\left(\frac{\partial \langle\psi_t^\omega|}{\partial\omega_i} \frac{\partial |\psi_t^\omega\rangle}{\partial\omega_j} - \frac{\partial \langle\psi_t^\omega|}{\partial\omega_i} |\psi_t^\omega\rangle \langle\psi_t^\omega| \frac{\partial |\psi_t^\omega\rangle}{\partial\omega_j} \right) \dot\omega_j$$
$$= -\text{Re}\left(\frac{\partial \langle\psi_t^\omega|}{\partial\omega_i} H |\psi_t^\omega\rangle \right). \tag{D10}$$

APPENDIX E: PROOF OF THEOREM 1

For $\delta_t > 0$, let the state evolution be defined with respect to the effective gradient given in Eq. (C7)

$$|\psi_{t+\delta_t}^\omega\rangle = |\psi_t^\omega\rangle + \delta_t |\dot\psi_t^{\dot\nu}\rangle$$
$$= |\psi_t^\omega\rangle + \delta_t\left(|\dot\psi_t^\omega\rangle - iE_t^\omega - i\text{Im}\left(\langle\dot\psi_t^\omega|\psi_t^\omega\rangle\right) |\psi_t^\omega\rangle\right). \tag{E1}$$

Combining Eq. (E1) with the triangle inequality gives

$$B\left(|\psi_{t+\delta_t}^\omega\rangle, |\psi_{t+\delta_t}^*\rangle\right) \leq B\left(|\psi_{t+\delta_t}^\omega\rangle, \left(\mathbb{1} - i\delta_t H\right) |\psi_t^\omega\rangle\right)$$
$$+ B\left(\left(\mathbb{1} - i\delta_t H\right) |\psi_t^\omega\rangle, |\psi_{t+\delta_t}^*\rangle\right). \tag{E2}$$

Using Eq. (B1) and neglecting terms of order $\mathcal{O}(\delta_t^2)$ gives

$$B\left(|\psi_{t+\delta_t}^\omega\rangle, \left(\mathbb{1} - i\delta_t H\right) |\psi_t^\omega\rangle\right)$$
$$= \min_{\phi\in[0,2\pi]} \left\| e^{i\phi}\left(|\psi_{t+\delta_t}^\omega\rangle\right) - \left(\mathbb{1} - i\delta_t H\right) |\psi_t\rangle \right\|_2$$
$$\leq \left\| |\psi_{t+\delta_t}^\omega\rangle - \left(\mathbb{1} - i\delta_t H\right) |\psi_t\rangle \right\|_2$$
$$= \delta_t \left\| |\dot\psi_t^\omega\rangle + i\left(H - E_t^\omega - \text{Im}(\langle\dot\psi_t^\omega|\psi_t^\omega\rangle)\right) |\psi_t^\omega\rangle \right\|_2$$
$$=: \delta_t \||e_t\rangle\|_2, \tag{E3}$$

where the penultimate step uses Eq. (C6).

For the second term in Eq. (E2), we employ a simplified notation for QRTE for a time step δ_t, i.e.,

$$\mathcal{P}_{\delta_t}^{\text{real}}\left(|\phi_t\rangle\right) := |\phi_{t+\delta_t}\rangle = \left(\mathbb{1} - iH\right) |\phi_t\rangle, \tag{E4}$$

which leads to

$$B\left(\left(\mathbb{1} - i\delta_t H\right) |\psi_t^\omega\rangle, |\psi_{t+\delta_t}^*\rangle\right) \tag{E5}$$
$$= B\left(\mathcal{P}_{\delta_t}^{\text{real}}\left(|\psi_t^\omega\rangle\right), \mathcal{P}_{\delta_t}^{\text{real}}\left(|\psi_{t+\delta_t}^*\rangle\right)\right) \tag{E6}$$
$$\leq B\left(|\psi_t^\omega\rangle, |\psi_{t+\delta_t}^*\rangle\right), \tag{E7}$$

The penultimate step uses that all physical processes are non-trace-increasing [26], which implies that the Bures metric does not increase either.

Combining Eqs. (E2), (E3), and (E5) gives

$$B\left(|\psi_{t+\delta_t}^\omega\rangle, |\psi_{t+\delta_t}^*\rangle\right) \leq B\left(|\psi_t^\omega\rangle, |\psi_t^*\rangle\right) + \delta_t \||e_t\rangle\|_2. \tag{E8}$$

Assuming that $B\left(|\psi_0\rangle, |\psi_0^*\rangle\right) = 0$, we can evolve

$$B\left(|\psi_T^\omega\rangle, |\psi_T^*\rangle\right) = \delta_t \sum_{k=0}^{K} \||e_{k\delta_t}\rangle\|_2, \tag{E9}$$

where K corresponds to the number of time steps. Finally setting $\delta_t = T/t$ leads to

$$B\left(|\psi_T^\omega\rangle, |\psi_T^*\rangle\right) \leq \int_0^T \||e_t\rangle\|_2 \, dt := \epsilon_T, \qquad \text{(E10)}$$

which proves the assertion. $\qquad \square$

APPENDIX F: PROOF OF THEOREM 2

Combining that Eq. (D7) gives

$$
\begin{aligned}
|\psi_{t+\delta_t}^\omega\rangle &= |\psi_t^\omega\rangle + \delta_t |\dot\psi_t^\nu\rangle \\
&= |\psi_t^\omega\rangle + \delta_t\left(|\dot\psi_t^\omega\rangle + i\,\text{Im}(\langle\dot\psi_t^\omega|\psi_t^\omega\rangle)|\psi_t^\omega\rangle\right), \quad \text{(F1)}
\end{aligned}
$$

with the triangle inequality for $\delta_t > 0$ results in

$$
\begin{aligned}
&B\left(|\psi_{t+\delta_t}^\omega\rangle, |\psi_{t+\delta_t}^*\rangle\right) \\
&\quad \leq B\left(|\psi_t^\omega\rangle + \delta_t|\dot\psi_t^\nu\rangle, \left(\mathbb{1} + \delta_t\left(E_t^\omega - H\right)\right)|\psi_t^\omega\rangle\right) \\
&\qquad + B\left(\left(\mathbb{1} + \delta_t\left(E_t^\omega - H\right)\right)|\psi_t^\omega\rangle, |\psi_{t+\delta_t}^*\rangle\right). \quad \text{(F2)}
\end{aligned}
$$

Next, we consider the two terms separately. Using Eq. (B1) and neglecting terms of order $\mathcal{O}(\delta_t^2)$ gives

$$
\begin{aligned}
&B\left(|\psi_t^\omega\rangle + \delta_t|\dot\psi_t^\nu\rangle, \left(\mathbb{1} + \delta_t\left(E_t^\omega - H\right)\right)|\psi_t^\omega\rangle\right) \\
&= \min_{\phi\in[0,2\pi]} \left\|e^{i\phi}(|\psi_t^\omega\rangle + \delta_t|\dot\psi_t^\nu\rangle)\right. \\
&\qquad \left. - \left(\mathbb{1} + \delta_t\left(E_t^\omega - H\right)\right)|\psi_t^\omega\rangle\right\|_2 \\
&\leq \left\||\psi_t^\omega\rangle + \delta_t|\dot\psi_t^\nu\rangle - \left(\mathbb{1} + \delta_t\left(E_t^\omega - H\right)\right)|\psi_t^\omega\rangle\right\|_2 \\
&= \delta_t\left\||\dot\psi_t^\nu\rangle - \left(E_t^\omega - H\right)|\psi_t^\omega\rangle\right\|_2 \\
&= \delta_t\left\||\dot\psi_t^\omega\rangle - \left(E_t^\omega - H - i\,\text{Im}\left(\langle\dot\psi_t^\omega|\psi_t^\omega\rangle\right)\right)|\psi_t^\omega\rangle\right\|_2 \\
&= \delta_t\,\||e_t\rangle\|_2, \quad \text{(F3)}
\end{aligned}
$$

where the penultimate step uses Eq. (D8).

For the second term in Eq. (F2), we employ a simplified notation for exact QITE for a time step δt, i.e.,

$$\mathcal{P}_{\delta t}^{\text{imag}}\left(|\phi_t\rangle\right) := |\phi_{t+\delta t}\rangle = \left(\mathbb{1}\langle\phi_t|H|\phi_t\rangle + H\right)|\phi_t\rangle, \quad \text{(F4)}$$

which leads to

$$B\left(\left(\mathbb{1} + \delta_t\left(E_t^\omega - H\right)\right)|\psi_t^\omega\rangle, |\psi_{t+\delta_t}^*\rangle\right) \qquad \text{(F5)}$$

$$= B\left(\mathcal{P}_{\delta t}^{\text{imag}}\left(|\psi_t^\omega\rangle\right), \mathcal{P}_{\delta t}^{\text{imag}}\left(|\psi_{t+\delta_t}^*\rangle\right)\right) \qquad \text{(F6)}$$

$$\leq B\left(|\psi_t^\omega\rangle, |\psi_{t+\delta_t}^*\rangle\right), \qquad \text{(F7)}$$

where the last line holds because all physical processes are non-trace-increasing [26].

Combining Eqs. (F2), (F3), and (F3) gives

$$B\left(|\psi_{t+\delta_t}^\omega\rangle, |\psi_{t+\delta_t}^*\rangle\right) \leq B\left(|\psi_t^\omega\rangle, |\psi_t^*\rangle\right) + \delta_t\,\||e_t\rangle\|_2. \quad \text{(F8)}$$

The final steps of the proof are equivalent to the ones presented in Appendix E. $\qquad \square$

APPENDIX G: VarQTE IMPLEMENTATION

The implementation of VarQTE relies on the evaluation of $\text{Im}(C_i - \partial\langle\psi_t^\omega|/\partial\omega_i|\psi_t^\omega\rangle E_t^\omega)$, $\text{Re}(C_i)$ and $\mathcal{F}_{ij}^Q$, which are introduced in Sec. II. The parameterized state is constructed as $|\psi_t^\omega\rangle = \prod_{p=0}^k U_p(\omega_p)|0\rangle^{\otimes n}$. Thus, we may use that parameterized unitaries can be written as $U_j(\omega_j) = e^{iM(\omega_j)}$, where $M(\omega_j)$ denotes a parameterized Hermitian matrix. To simplify the notation, we assume that $M(\omega_j) = -\omega_j/(2)\sigma_j$ for $\sigma_j \in \{\mathbb{1}, X, Y, Z\}$. Since

$$\frac{\partial U_j(\omega_j)}{\partial\omega_j} = -\frac{i}{2}\sigma_j U_j(\omega_j), \qquad \text{(G1)}$$

it follows that

$$\frac{\partial|\psi_t^\omega\rangle}{\partial\omega_j} = -\frac{i}{2}\prod_{p=j+1}^k U_p(\omega_p)\sigma_j U_j(\omega_j)\prod_{p=0}^{j-1} U_p(\omega_p)|0\rangle^{\otimes n}. \quad \text{(G2)}$$

Next, we employ Eq. (G2) to find that

$$C_i = -\frac{i}{2}\langle\psi_t^\omega|H\prod_{p=j+1}^k U_p\sigma_j U_j\prod_{p=0}^{j-1} U_p|0\rangle^{\otimes n}, \qquad \text{(G3)}$$

as well as,

$$\frac{\partial\langle\psi_t^\omega|}{\partial\omega_i}|\psi_t^\omega\rangle = \frac{i}{2}\langle 0|^{\otimes n}\prod_{p=0}^{j-1} U_p^\dagger U_j^\dagger\sigma_j\prod_{p=j+1}^k U_p^\dagger|\psi_t^\omega\rangle, \quad \text{(G4)}$$

and

$$
\begin{aligned}
\mathcal{F}_{ij}^Q &= \frac{1}{4}\text{Re}\Big(\langle 0|^{\otimes n}\prod_{p=0}^{i-1} U_p^\dagger U_i^\dagger\sigma_i\prod_{p=i+1}^{j-1} U_p^\dagger\sigma_j\prod_{p=0}^{j-1} U_p|0\rangle^{\otimes n} \\
&\qquad - \langle 0|^{\otimes n}\prod_{p=0}^{i-1} U_p^\dagger U_i^\dagger\sigma_i\prod_{p=i+1}^k U_p^\dagger|\psi_t^\omega\rangle\langle\psi_t^\omega| \\
&\qquad \times \prod_{p=j+1}^k U_p\sigma_j U_j(\omega_j)\prod_{p=0}^{j-1} U_p|0\rangle^{\otimes n}\Big), \quad \text{(G5)}
\end{aligned}
$$

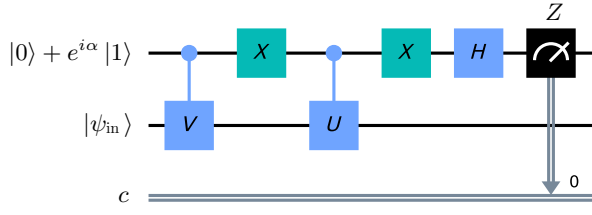where we assume that $i < j$ and simplify the notation with $U_p := U_p(\omega_p)$.

FIG. 12. This quantum circuit—originally proposed in Ref. [36]—uses an additional working qubit to evaluate $\mathrm{Re}\left(\mathrm{e}^{i\alpha}\left\langle\psi_{\mathrm{in}}\right|U^{\dagger}V\left|\psi_{\mathrm{in}}\right\rangle\right)$. Notably, this requires only measurement of the working qubit with respect to Z.

One can, now, see that $\mathrm{Im}(C_i - \partial\left\langle\psi_t^{\omega}\right|/\partial\omega_i\left|\psi_t^{\omega}\right\rangle E_t^{\omega})$, $\mathrm{Re}(C_i)$, and $\mathcal{F}_{ij}^{Q}$ may be decomposed into terms of the form $\mathrm{Re}(\mathrm{e}^{i\alpha}\left\langle\psi_{\mathrm{in}}\right|UV\left|\psi_{\mathrm{in}}\right\rangle)$, respectively $\mathrm{Re}(\mathrm{e}^{i\alpha}\left\langle\psi_{\mathrm{in}}\right|HV\left|\psi_{\mathrm{in}}\right\rangle)$ using that $\mathrm{Im}(iz) = \mathrm{Re}(z)$. We can, thus, evaluate the equations either with the quantum circuit shown in Fig. 12 or the one presented in Fig. 13.

Consider, for example, $\left|\psi_t^{\omega}\right\rangle = \mathrm{e}^{-i\frac{\omega_1}{2}X}\,\mathrm{e}^{-i\frac{\omega_0}{2}Y}\left|0\right\rangle$. Then,

$$\frac{\partial\left\langle\psi_t^{\omega}\right|}{\partial\omega_1}\left|\psi_t^{\omega}\right\rangle = \frac{i}{2}\left\langle\psi_t^{\omega}\right|X\left|\psi_t^{\omega}\right\rangle, \qquad \text{(G6)}$$

and

$$C_1 = -\frac{i}{2}\left\langle\psi_t^{\omega}\right|HX\left|\psi_t^{\omega}\right\rangle. \qquad \text{(G7)}$$

To evaluate $\mathrm{Im}(\partial\left\langle\psi_t^{\omega}\right|/\partial\omega_1\left|\psi_t^{\omega}\right\rangle)$ with the circuit shown in Fig. 12, we set $\alpha = -\pi$, $\left|\psi_{\mathrm{in}}\right\rangle = \left|\psi_t^{\omega}\right\rangle$, $V = X$ and $U = \mathbb{1}$. Furthermore, $\mathrm{Im}(C_1)$, respectively, $\mathrm{Re}(C_1)$ can be computed using Fig. 13 with $\alpha = 0$, respectively, $\alpha = -\pi/2$, $\left|\psi_{\mathrm{in}}\right\rangle = \left|\psi_t^{\omega}\right\rangle$ and $V = X$. Similarly, the evaluation of

$$\begin{aligned}\mathcal{F}_{01}^{Q} &= \frac{1}{4}\mathrm{Re}\Big(\left\langle 0\right|\mathrm{e}^{i\frac{\omega_0}{2}Y}YX\,\mathrm{e}^{-i\frac{\omega_0}{2}Y}\left|0\right\rangle \\ &\quad - \left\langle 0\right|Y\left|0\right\rangle\left\langle 0\right|\mathrm{e}^{i\frac{\omega_0}{2}Y}X\,\mathrm{e}^{-i\frac{\omega_0}{2}Y}\left|0\right\rangle\Big) \\ &= \mathrm{Re}\Big(\left\langle 0\right|\mathrm{e}^{i\frac{\omega_0}{2}Y}YX\,\mathrm{e}^{-i\frac{\omega_0}{2}Y}\left|0\right\rangle\Big). \qquad \text{(G8)}\end{aligned}$$
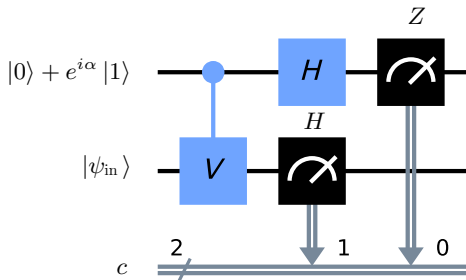
FIG. 13. This quantum circuit uses an additional working qubit to evaluate $\mathrm{Re}(\mathrm{e}^{i\alpha}\left\langle\psi_{\mathrm{in}}\right|HV\left|\psi_{\mathrm{in}}\right\rangle)$, where the working qubit is measured with respect to Z and the state $\left|\psi_{\mathrm{in}}\right\rangle$ with respect to the observable H.
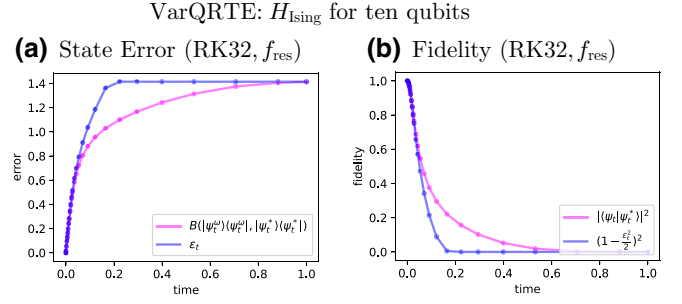

FIG. 14. VarQRTE for $\left|\psi_0\right\rangle = \mathrm{e}^{-i\alpha}\left|0\right\rangle^{\otimes 10}$, H_{Ising} and $T = 1$ with RK32 is based on the residual ODE. (a) shows the error bounds ϵ_t and the actual Bures metric. (b) illustrates the corresponding fidelity and fidelity bound.

may be conducted with the setup illustrated in Fig. 12 using $\alpha = 0$, $\left|\psi_{\mathrm{in}}\right\rangle = \mathrm{e}^{-i\frac{\omega_0}{2}Y}\left|0\right\rangle$, $V = X$ and $U = Y$.

APPENDIX H: LARGER ISING MODEL SIMULATIONS

To rule out that the utility of the presented error bounds is limited to systems consisting only of a few qubits, experiments for larger system dimensions have to be conducted. To improve our understanding of the method's scalability, the experimental analysis of our model is extended to the Ising model described in Sec. IV with ten qubits. More specifically, we run VarQRTE and VarQITE simulations for $T = 1$ using a Runge-Kutta method of order 3(2) (RK32) from SciPy [31]. Figure 14 shows the results of the VarQRTE experiment that employs the residual ODE and ridge regression to solve the underlying SLE. We can see that the error bound matches the actual error up to a factor 10^{-1} until the Bures distance reaches approximately 0.8. This directly relates to a fidelity of 0.68. In the VarQITE setup, the propagation is based on the error-based ODE and the respective SLE is solved with a least-squares approach. The results are presented in Fig. 15. The plots show that the ODE solver requires many time steps indicating a volatile
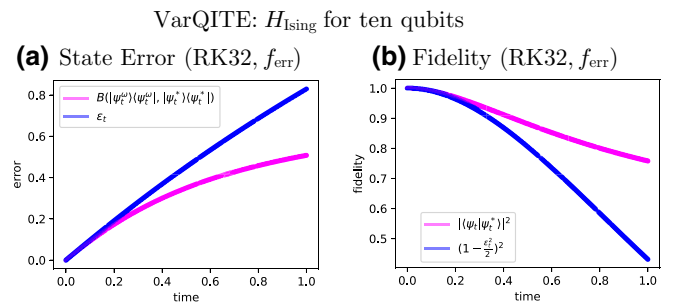

FIG. 15. VarQITE for $\left|\psi_0\right\rangle = \mathrm{e}^{-i\alpha}\left|0\right\rangle^{\otimes 10}$, H_{Ising}, and $T = 1$ with RK32 is based on the error-based ODE. (a) shows the error bounds ϵ_t and the actual Bures metric. (b) illustrates the corresponding fidelity and fidelity bound.

propagation. The resulting error bounds then diverge by more than a factor 10^{-1} when the Bures distance reaches 0.35, which corresponds to a fidelity of 0.94.

———————

[1] T. S. Cubitt, A. Montanaro, and S. Piddock, Universal quantum Hamiltonians, Proc. Natl. Acad. Sci. **115**, 9497 (2018).

[2] R. Barends, L. Lamata, J. Kelly, L. García-Álvarez, A. G. Fowler, A. Megrant, E. Jeffrey, T. C. White, D. Sank, and J. Y. Mutus, Digital quantum simulation of fermionic models with a superconducting circuit, Nat. Commun. **6**, 7654 (2015).

[3] A. Smith, M. S. Kim, F. Pollmann, and J. Knolle, Simulating quantum many-body dynamics on a current digital quantum computer, Npj Quantum Inf. **5**, 106 (2019).

[4] S. Barison, F. Vicentini, and G. Carleo, An efficient quantum algorithm for the time evolution of parameterized circuits, Quantum **5**, 512 (2021).

[5] J. Kempe, A. Kitaev, and O. Regev, The complexity of the local Hamiltonian problem, SIAM J. Comput. **35**, 9497 (2006).

[6] S. McArdle, T. Jones, S. Endo, Y. Li, S. C. Benjamin, and X. Yuan, Variational ansatz-based quantum simulation of imaginary time evolution, Npj Quantum Inf. **5**, 75 (2019).

[7] F. Fontanela, A. Jacquier, and M. Oumgari, Short communication: A quantum algorithm for linear PDEs arising in finance, SIAM J. Financial Math. **12**, SC98 (2021).

[8] K. Kubo, Y. O. Nakagawa, S. Endo, and S. Nagayama, Variational quantum simulations of stochastic differential equations, Phys. Rev. A **103**, 052425 (2021).

[9] C. Zoufal, A. Lucchi, and S. Woerner, Variational quantum Boltzmann machines, Quantum Mach. Intell. **3**, 7 (2021).

[10] X. Yuan, S. Endo, Q. Zhao, Y. Li, and S. C. Benjamin, Theory of variational quantum simulation, Quantum **3**, 191 (2019).

[11] M. Motta, C. Sun, A. T. K. Tan, M. J. O'Rourke, E. Ye, A. J. Minnich, F. G. S. L. Brandão, and G. K.-L. Chan, Determining eigenstates and thermal states on a quantum computer using quantum imaginary time evolution, Nat. Phys. **16**, 205 (2020).

[12] K. Temme, T. J. Osborne, K. G. H. Vollbrecht, D. Poulin, and F. Verstraete, Quantum Metropolis sampling, Nature **471**, 87 (2011).

[13] M.-H. Yung and A. Aspuru-Guzik, A quantum–quantum Metropolis algorithm, Proc. Natl. Acad. Sci. **109**, 754 (2012).

[14] J. Gacon, C. Zoufal, G. Carleo, and S. Woerner, Simultaneous perturbation stochastic approximation of the quantum Fisher information, Quantum **5**, 567 (2021).

[15] S. Lloyd, Universal quantum simulators, Science **273**, 1073 (1996).

[16] Y. Li and S. C. Benjamin, Efficient variational quantum simulator incorporating active error minimization, Phys. Rev. X **7**, 021050 (2017).

[17] S. Endo, J. Sun, Y. Li, S. C. Benjamin, and X. Yuan, Variational quantum simulation of general processes, Phys. Rev. Lett. **125**, 010501 (2020).

[18] P. A. M. Dirac, Note on exchange phenomena in the Thomas atom, Math. Proc. Camb. Philos. Soc. **26**, 376 (1930).

[19] R. Martinazzo and I. Burghardt, Local-in-time error in variational quantum dynamics, Phys. Rev. Lett. **124**, 150601 (2020).

[20] A. McLachlan, A variational solution of the time-dependent Schrödinger equation, Mol. Phys. **8**, 39 (1964).

[21] R. Tahir-Kheli, *Ordinary Differential Equations : Mathematical Tools for Physicists* (Springer International Publishing, Cham, 2018).

[22] H. H. S. Chan, R. Meister, T. Jones, D. P. Tew, and S. C. Benjamin, Grid-based methods for chemistry simulations on a quantum computer, Sci. Adv. **9**, eabo7484 (2023).

[23] S. L. Braunstein and C. M. Caves, Statistical distance and the geometry of quantum states, Phys. Rev. Lett. **72**, 3439 (1994).

[24] J. J. Meyer, Fisher information in noisy intermediate-scale quantum applications, Quantum **5**, 539 (2021).

[25] Z.-J. Zhang, J. Sun, X. Yuan, and M.-H. Yung, Low-depth Hamiltonian simulation by an adaptive product formula, Phys. Rev. Lett. **130**, 040601 (2023).

[26] M. A. Nielsen and I. L. Chuang, *Quantum Computation and Quantum Information* (Cambridge University Press, Cambridge, 2010).

[27] M. Hayashi, *Quantum Information: An Introduction* (Springer Berlin Heidelberg, Berlin, Heidelberg, 2006).

[28] H. Abraham, T. Alexander, P. Barkoutsos, L. Bello, Y. Ben-Haim, D. Bucher, F. J. Cabrera-Hernández, J. Carballo-Franquis, A. Chen, C.-F. Chen *et al.*, Qiskit: An open-source framework for quantum computing, (2019). Available online https://github.com/Qiskit.

[29] P. Calabrese, F. H. L. Essler, and M. Fagotti, Quantum quench in the transverse field Ising chain: I. Time evolution of order parameter correlators, J. Stat. Mech.: Theory Exp. **7**, P07016 (2012).

[30] D. F. Griffiths and D. J. Higham, *Numerical Methods for Ordinary Differential Equations: Initial Value Problems* (Springer London, London, 2010).

[31] P. Virtanen, R. Gommers, T. E. Oliphant, M. Haberland, T. Reddy, D. Cournapeau, E. Burovski, P. Peterson, W. Weckesser, J. Bright *et al.*, SciPy 1.0: Fundamental algorithms for scientific computing in Python, Nat. Methods **17**, 261 (2020).

[32] C. R. Harris, K. J. Millman, S. J. van der Walt, R. Gommers, P. Virtanen, D. Cournapeau, E. Wieser, J. Taylor, S. Berg, N. J. Smith *et al.*, Array programming with NumPy, Nature **585**, 357 (2020).

[33] F. Pedregosa *et al.*, Scikit-learn: Machine learning in Python, J. Mach. Learn. Res. **12**, 2825 (2011), Available online https://scikit-learn.org/.

[34] Qiskit https://github.com/Qiskit/qiskit-terra/tree/main/qiskit/opflow/gradients.

[35] D. C. McKay, C. J. Wood, S. Sheldon, J. M. Chow, and J. M. Gambetta, Efficient Z gates for quantum computing, Phys. Rev. A **96**, 022330 (2017).

[36] R. Somma, G. Ortiz, J. E. Gubernatis, E. Knill, and R. Laflamme, Simulating physical phenomena by quantum networks, Phys. Rev. A **65**, 042323 (2002).